Pillaring Puckered Layer Silicates

Zengqun Deng, Jean-François H. Lambert, and José J. Fripiat*

Department of Chemistry and Laboratory for Surface Studies, University of Wisconsin—Milwaukee, P. O. Box 413, Milwaukee, Wisconsin 53201

Received April 20, 1989

Upon acid leaching or alkylammonium intercalation, $KHSi_2O_5$ is transformed into a silicic acid or a silicic acid intercalate, where in the structure pairs of SiO_4 tetrahedra are alternately pointing on both sides of the basal hexagonal network of oxygens. A fraction of the layers is bound by siloxane bridges as shown by ^{29}Si MAS NMR, resulting in an interstratified structure. Pillaring with aluminum polyhydroxy polymers yields an interstratification of open and siloxane-bridged galleries having a surface area as high as 400 m^2/g after drying at 100 °C and 200 m^2/g after calcination at 500 °C. The galleries opened by the aluminum polyhydroxy polymers have cross sections between 10 and 30 Å and their volume is on the order of 0.12 mL/g in the favorable cases. High-resolution ^{27}Al magic-angle-spinning (MAS) NMR detects three distinct resonance lines corresponding to three kinds of aluminum sites. One is a "framework" tetrahedral Al within a Si $Q^4(1Al)$ environment. The other two lines at 0 and 30 ppm belong to "nonframework" aluminum. The 0 ppm line is that of octahedral Al, whereas the third resonance at ~30 ppm may be assigned either to strongly distorted tetrahedral Al or to pentacoordinated Al. The pillaring mechanism, which is very different from that observed for clay minerals, is discussed.

Introduction

Pillaring, or intercalation of inorganic oligomers into layered materials, offers the possibility of designing new classes of porous structures for shape-selective intracrystalline catalysis. Such zeolite-like materials are easily obtained from the pillaring of clay minerals, and they have attracted a lot of interest.[1-5] The most commonly used pillar in this case is the aluminum polymer $Al_{13}O_4(OH)_{24}(H_2O)_{12}$, abbreviated as Al_{13}. It has been intercalated in structures where the lattice charge originates in substitutions in the octahedral layers, such as montmorillonite,[4] as well as in tetrahedrally substituted clays, such as beidellite.[6-8] In the latter case, the charge localization seems to result in a better organization of the pillars. In order to extend the knowledge on pillared structures beyond clay materials, we chose the crystalline layered silicate $KHSi_2O_5$ as a candidate for Al pillaring.

In a recent paper,[9] we have shown that the hydrolysis product of $KHSi_2O_5$ has a formula of $H_{2(1-x)}Si_2O_{5-x}\cdot yH_2O$ ($x > 0$) rather than $H_2Si_2O_5$ as proposed before.[10-12] ^{29}Si NMR indicates the presence of silicon in both Q^3 and Q^4 environments with variable Q^4/Q^3 ratios, while the original $KHSi_2O_5$ exhibited only Q^3 silicon, and we proposed a rough structure sketch to account for these observations. We also studied alkylammonium-intercalated $KHSi_2O_5$, in which potassium is completely removed by alkylammonium. Hydrolyzed as well as alkylammonium intercalated products have surface areas of about 20–30 m^2/g.

The present paper is concerned with aluminum polymer pillaring of $KHSi_2O_5$, either by direct exchange (of the potassium salt) or indirect exchange (through the alkylammonium intercalate). We used surface area measurements, X-ray diffraction, and magic-angle-spinning (MAS) NMR spectroscopy to study the pillared products. A possible pillaring mechanism is proposed, and the thermal stability of the pillared product is discussed.

Experimental Section

(1) Preparation of Interlayered Cations. Two different aluminum polyhydroxy polymer solutions have been used. We first synthesized aluminum polyhydroxy chloride polymer solutions according to Schoenherr et al.[13] To 250 mL of a 0.4 M solution of $AlCl_3\cdot 6H_2O$, 750 mL of a 0.26 M solution of NaOH is added dropwise over a period of several hours, followed by aging at 60 °C for 2 h. Then a solution of an excess quantity of Na_2SO_4 is added at room temperature (RT) and left to react for 48 h, which causes the sulfate of the aluminum polyhydroxy polymer to precipitate. The precipitate is collected by centrifugation, washed, and reacted with a $BaCl_2$ solution, yielding a solution of pure (Na^+-free) Al_{13} chloride. This procedure is necessary because the Na^+ ions can give rise to a competing ion-exchange reaction during the pillaring. We also used the commercial Chlorhydrol 50% solution provided by the Reheis Chemical Company (prepared by acid hydrolysis of Al metal) after dilution to a total Al concentration of 0.2 M and aging either at RT for several days or at 60 °C for 2 h; this solution is later referred to as ACH.

(2) Intercalation. $KHSi_2O_5$ was prepared by hydrothermal synthesis at 300 °C in the same way as in ref 9.

This product was exchanged three times with a 1 M alkylammonium chloride solution (N/Si ratio = 10) to yield the intercalates $(RNH_3)_{2z}H_{2(1-x-z)}Si_2O_{5-x}\cdot yH_2O$, where $z \approx 0.15$, as described in ref 9. Alternatively, ethylammonium fluoride exchange was carried out in the same way, in the presence of small excesses of HF (pH = 5–6.5) to investigate the possible effect of OH^-/F^- substitution in the lattice.

Aluminum pillaring was effected in either of two ways.

(a) Direct Exchange. In this procedure, the original $KHSi_2O_5$ was suspended in the ACH solution under stirring and then centrifuged and washed several times. The exchange conditions were varied without any appreciable influence on the final results: the number of exchanges varied from 1 to 3, the contact time for each exchange from 1 h to 4 days, the exchange temperature from RT to 90 °C, and the Al/K^+ ratio from 1 to 40. Samples prepared in this way are labeled as D samples: the experimental conditions for two of them are listed in Table I.

(b) Indirect Exchange. In this case, alkylammonium-intercalated $KHSi_2O_5$, with at least 95% K^+ elimination, was used immediately after preparation to prevent destruction of the intercalate by alkylamine evaporation (this happens in less than

(1) Brindley, G. W.; Kao, C. C. *Clays Clay Miner.* **1980**, *28*, 435.
(2) Brindley, G. W.; Sempels, R. E. *Clays Clay Miner.* **1977**, *12*, 229.
(3) Occelli, M. L.; Finseth, D. H. *J. Catal.* **1980**, *99*, 316.
(4) Pinnavaia, T. J. *Science* **1983**, *220*, 4595.
(5) Vaughan, D. E. W.; Lussier, R. J. *5th Inter. Conf. on Zeolites*: Rees, L. V. C., Ed.; Heyden: Philadelphia, 1980; p 94.
(6) Plee, D.; Borg, F.; Schutz, A.; Poncelet, G.; Fripiat, J. J. *J. Am. Chem. Soc.* **1985**, *107*, 2326.
(7) Schutz, A.; Plee, D.; Poncelet, G.; Fripiat, J. J. *Catalysis by acids and Bases*: Imelik, B., Ed.; Elsevier: Amsterdam, 1985; p 343.
(8) Schutz, A.; Plee, D.; Borg, F.; Jacobs, P. A.; Poncelet, G.; Fripiat, J. J. *Proc. 8th Intern. Clay Conf., Denver, 1985*; Schulz, L. G., et al., Eds.; The Clay Mineral Society: Denver, 1985; p 305.
(9) Deng, Z. Q.; Lambert, J.-F.; Fripiat, J. J. *Chem. Mater.* **1989**, *1*, 375.
(10) Le Bihan, M.-T.; Kalt, A.; Wey, R. *Bull. Soc. Fr. Minéral. Cristallogr.* **1971**, *94*, 15.
(11) Kalt, A.; Wey, R. *Bull. Groupe Fr. Argiles* **1968**, *20*, 205.
(12) Liebau, F. *Z. Kristallogr.* **1964**, *120*, 427.
(13) Schönherr, S.; Görz, H.; Müller, D.; Gessner, W. *Z. Anorg. Allg. Chem.* **1981**, *476*, 188.

0897-4756/89/2801-0640$01.50/0

Table I. Preparation Procedures and Surface Areas for Several Representative Samples[e]

	Al intercalation conditions					
sample	R(Al)	T, °C	time, h	no. of exchanges	T_{pret}, °C	A, m^2/g
$KHSi_2O_5$[a]	0			0	100	<0.2
"HP"[a]	0			0	100	24
		D Series: Direct Exchange				
D-31	180	60	20	1	100	87.3
D-32	90	25	24	3	100	139.2
					500	59.8
I Series: From the Ethylammonium Chloride Intercalate; pH ~5						
I-10 (W)[c]	180	25	24	1[b]	100	105.4
					200	97.4
					300	97.1
I-19 (UW)	120	25	16	1	150	162.5
					500	60.8
I-20 (UW)	60	25	100	1	100	189.5
					300	78
					500	60
I-24 (W)	120	90	3	1	150	159.7
					300	67
I-40 (W)[c]	1200	25	24	1	100	186.4
					300	122.5
I-42 (UW)[d]	180	25	24	1	100	303
					300	263
IF Series: From the Ethylammonium Fluoride Intercalate; pH Specified						
IF-11 (UW) (pH = 5)	180	25	24	1	100	314.7
IF-12 (UW) (pH = 5.5)	180	25	24	1	100	497.7
					300	406
IF-13 (UW) (pH = 5.8)	180	25	24	1	100	470
					300	408
					500	367
IF-14 (UW) (pH = 6.5)	180	25	24	1	100	288.8
IF-04 (W) (pH = 6)	180	25	24	1	100	226
					300	217
IF-41 (W) (pH = 6)[c]	180	25	24	1	100	230.3
					300	218

[a] From ref 9. "HP" = $KHSi_2O_5$ hydrolysis product. [b] Sample I-10 was prepared from a solution of pure Al_{13} (see Experimental Section)—all other samples from ACH. [c] Samples submitted to chemical analysis. [d] pH of the ethylammonium chloride solution: 2.5. [e] For series I and IF, the solid sample was obtained by centrifugation after the ethylammonium intercalation step. Samples submitted to further washing prior to contact with the pillaring solution are indicated by W, samples used without further washing by UW. R(Al) is the nominal concentration of the aluminum polymer (either Al_{13} or ACH) expressed in milliequivalents of Al^{3+} per gram of starting material. A is the surface area after pretreatment at a temperature T_{pret}.

1 day for dried shorter chain intercalates; however, wet intercalates are more stable) and exchanged with either pure Al_{13} or ACH solutions. After the exchange, the products were centrifuged and vigorously washed. The experimental conditions were also varied in a broad range. The contact time, the Al/Si ratio, and the exchange temperature were systematically studied. Again the results depended little on these parameters. These samples are labeled as the I series in Table I.

(3) X-ray Diffraction. XRD patterns were obtained, with Cu Kα radiation, on a home-computerized Phillips diffractometer from either oriented films or powder samples. The oriented films were prepared by depositing the wet solids (after washing) on glass slides.

(4) N_2 Physical Adsorption. Surface areas were obtained from N_2 adsorption at 77 K according to the BET equation. These surface areas should be considered as approximations, because the N_2 adsorption isotherms do not belong strictly speaking to Brunauer's class II. Therefore, complete N_2 adsorption–desorption isotherms were measured for seven representative samples in the relative pressure range $0.01 \leq P/P_0 \leq 0.95$ in order to gain information on pore size distributions.

(5) Elemental Analysis. Elemental analyses effected by Galbraith Laboratories (Knoxville, TN) on three samples gave the following results: for I-10, $Al_{0.21}Si_2O_{4.315}(H_2O)_{2.18}$; for I-40, $Al_{0.14}Si_2O_{4.21}(H_2O)_{1.75}$; for IF-41, $Al_{0.054}Si_2O_{4.033}F_{0.048}(H_2O)_{0.892}$.

(6) MAS NMR. Magic-angle-spinning NMR spectra were recorded on a GN 500 spectrometer, in a magnetic field of 11.7 T. In such a field, the position of the ^{29}Si resonance is 99.3 MHz; that of the ^{27}Al resonance is 130.3 MHz. Samples were spun at the magic angle with frequencies of 6–9 kHz. Typical values of the acquisition parameters were as follows.

For ^{29}Si, the rf power was 60 or 500 W with pulse lengths of 7 or 3 μs, the number of acquisitions was 2000–10000, the acquisition time was 25 ms with proton decoupling, and the delay time was 1 s. Cross-polarization experiments were carried out with contact times of 3 ms.

For ^{27}Al, the rf power was 60 W, the pulse length was 2–5 μs, the number of acquisitions was 1000, the acquisition time was 51 ms, and the delay time was 0.5–1 s. The spectra of IF-41 were obtained with a rf power of 500 W and a pulse length of 0.5 μs.

(7) Scanning Electron Microscopy (SEM). Three samples, namely, the acid hydrolysis product of $KHSi_2O_5$(HP), and two samples pillared through the indirect exchange process, I-42 and IF-13, were examined after gold–palladium plating at magnifications between 2000 and 10000 (Jeol 8408).

Results

XRD. The XRD spectra of the initial salt $KHSi_2O_5$ and, for reference, of its hydrolysis product HP are described in ref 9.

The spectrum of ACH-exchanged sample D-31 after drying at RT exhibits, besides a broad band centered at around 15 Å, peaks at ~6, 4.30, 4.10, and 3.75 Å. The peaks at 6 and 3.75 Å are clear remnants of the hydrolysis product, corresponding to the 020 and 200 reflections, respectively, in the indexation of Le Bihan et al.:[10,11] their intensities are correlated (Table II), and they disappear upon heating at moderate temperatures, a fact compatible with the low thermal stability of HP. The ~4.30- and ~4.10-Å peaks are probably not reflections of the HP phase, since they are uncorrelated with the first two and rather stable upon heating. They are also observable in calcined HP and could be due to the "collapsed" siloxane-bridged phase that results from HP layer condensation (see ref 9). In particular, the 4.10-Å peak might correspond to a 200 reflection of the collapsed structure, since its spacing corresponds to a $KHSi_2O_5$ reflection of 200. However, 0k0 reflections (corresponding to the direction perpendicular to the layers) are not observable: it is assumed that the collapsed HP phase as well as the intercalates consists of random interstratifications (see Discussion section and ref 9).

The powder spectrum of D-32 is similar to that of D-31 except for the absence of the broad band at ~15 Å. Calcination at 500 °C also results in the disappearance of the 6- and ~3.75-Å peaks, while the reflection at ~4.10 Å is maintained longer. A small peak is apparent at 3.80–3.84 Å after calcination, but we think it is different from the original 3.75-Å reflection. It is rather close to the $KHSi_2O_5$ 111 reflection (d_{th} = 3.899 Å).

Provided the ACH solution is used, the XRD patterns of indirect-exchange products are very similar to those obtained from direct exchange. Typical spectra are shown in Figure 1. Figure 1a shows the XRD spectrum of the initial ethylammonium intercalate and of one of its ACH-exchange products, sample I-20, after RT drying (Figure 1b), drying at 70 °C overnight (Figure 1c), calcination at 300 °C for 2 h (Figure 1d), calcination at 400 °C for 1 h (Figure 1e), and finally calcination at 500 °C for 2 h (Figure 1f). The gradual disappearance of the 3.74-Å peak (HP 200) and the faster disappearance of the ~6-Å peak (HP 020) are well evidenced here. Again, a weak peak at

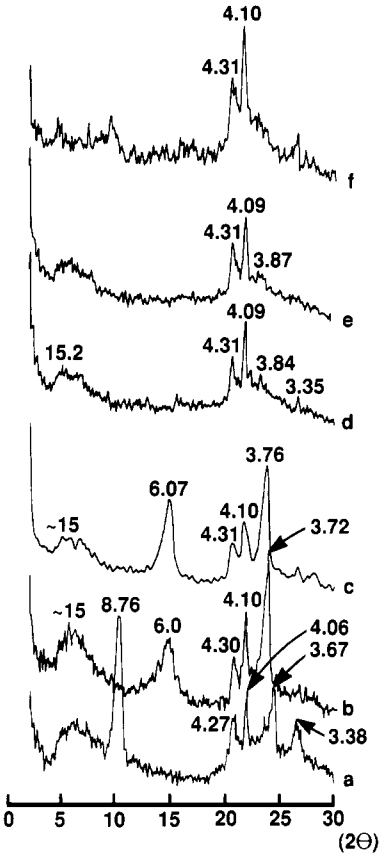

Figure 1. X-ray diffractograms, Cu Kα radiation, oriented films, of (a) $(C_2H_5NH_3^+)_{0.3}H_{1.7-2x}O_{5-x}\cdot yH_2O$, the ethylammonium intercalate used as the intermediate for indirect exchange in the I series; (b) indirect-exchange product I-20, after RT drying; and (c) I-20, after 12-h drying at 70 °C, (d) after 2-h calcination at 300 °C, (e) after 2 h at 400 °C, and (f) after 2 h at 500 °C.

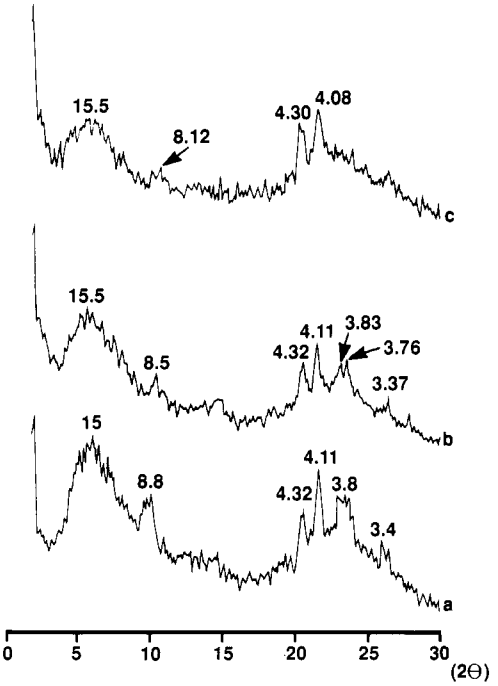

Figure 2. X-ray diffractograms, Cu Kα radiation, oriented films, of (a) IF-41, product of indirect exchange of the ethylammonium fluoride intercalate, after RT drying; (b) IF-41, after 12 h drying at 100 °C; and (c) IF-41, after 2 h at 300 °C.

3.8–3.85 Å is observable after calcination.

Sample I-40, which was prepared from ACH under somewhat different conditions from sample I-20 (see Table I), exhibited the same behavior.

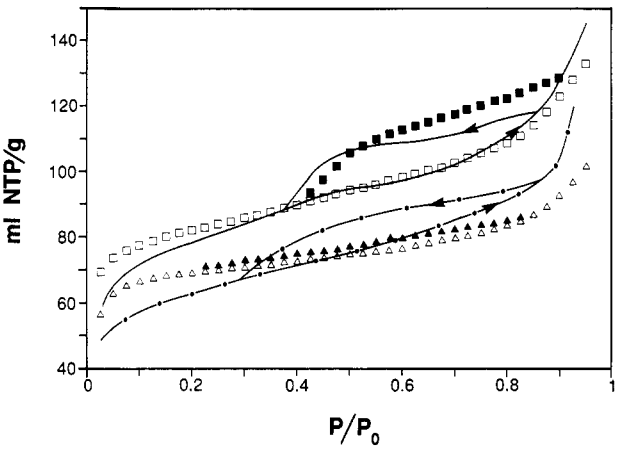

Figure 3. N_2 adsorption (→ and open symbols) and desorption (← and filled symbols) isotherms measured at 77 K on samples IF-13 (top solid line), IF-12 (■), I-42 (△), and IF-04 (bottom solid line) calcined at 300 °C for 2 h.

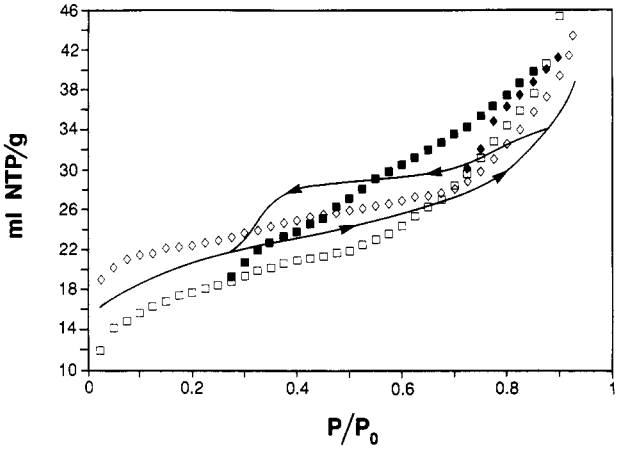

Figure 4. N_2 adsorption (→ and open symbols) and desorption (← and filled symbols) isotherms measured at 77 K on samples I-24 (■), I-20 (solid line), and I-40 (◇).

Figure 2 illustrates the evolution with increasing temperatures of an intercalate obtained from ethylammonium fluoride and contacted with ACH, IF-41. In this case, a weak broader peak is present at ~9 Å, and it is only for sample IF-41 that the reflections at 4.3 and 4.1 Å are observed. For other IF series samples, the best defined reflection is at ~3.7 Å (not shown).

Surface Areas and Porosity. Typical adsorption–desorption isotherms are shown in Figures 3 and 4. The two relative pressures (P/P_0) at which the hysteresis loop intersects the adsorption branch are of great physical significance. Beyond the upper values of P/P_0, capillary condensation occurs in macropores with radii ≥ 100 Å. Below the lower value of P/P_0, physical adsorption takes place, according to the BET model, with a limited, and small, number of molecular layers. The pore radii corresponding to the upper and lower limits of P/P_0, can be approximated by the procedure reviewed by Gregg and Sing.[14] At a specific value of P/P_0, the pore radius, r_p, is the sum of the average thickness of the adsorbed layer, t, and the pore radius, r_K, obtained from the Kelvin equation. the validity of the procedure becomes very uncertain when $t \approx r_K$, that is, for $P/P_0 \leq 0.3$. If V is the volume of N_2 adsorbed at the onset of the hysteresis loop

(14) Gregg, S. J.; Sing, K. S. W. *Adsorption, Surface area and Porosity*; Academic Press: New York, 1967; p 223.

Table II. Positions (Roman) and Approximate Intensities (Italicized) of the Main XRD Peaks

$KHSi_2O_5$			6.30		4.086	3.91		3.42
(powder)			*3.51*		*4.14*	*11.9*		*6.87*
HP	16		5.91		4.07		3.74	3.34
RT	*1.06*		*4.25*		*0.85*		*8.56*	*0.85*
HP dried	14			4.32	4.10	3.81		3.35
100 °C, 3 h	*0.51*			*0.94*	*1.98*	*0.43*		*0.34*
HP	14			4.34	4.12			3.36
2 h, 300 °C	*0.47*			*0.74*	*1.67*			*0.35*
D-31	16		5.97	4.30	4.10		3.75	(3.35)
RT	*0.64*		*1.49*	*0.49*	*1.55*		*3.09*	*0.43*
D-32			5.99	4.29	4.10		3.75	
RT (powder)			*1.22*	*0.57*	*0.97*		*2.87*	
D-32	14			4.27	4.09	3.83		
500 °C, 1 h	*<0.5*			*0.62*	*1.10*	*0.30*		
D-32	15			4.27	4.09	3.83		3.35
500 °C, 2 h	*0.78*			*0.43*	*0.78*	*0.29*		*0.25*
I-20	15		6.01	4.30	4.08		3.74	
RT	*0.85*		*1.23*	*0.98*	*1.60*		*2.92*	
I-20	15		6.07	4.31	4.10		3.76	
70 °C	*0.68*		*2.41*	*0.77*	*1.20*		*3.10*	
I-20	17			4.31	4.09	3.84		3.35
300 °C	*0.69*			*1.22*	*2.25*	*0.49*		*0.39*
I-20	16			4.31	4.09	(3.87)		
400 °C	*0.77*			*1.35*	*1.92*	*0.38*		
I-20	9.4			4.35	4.12			3.37
500 °C	0.53			*1.18*	*2.11*			*0.32*
I-24	16			4.36		~3.8		
RT	*0.44*			*0.65*		*0.61*		
I-40	15		~6	4.33	4.10		3.75	
RT	*1.07*		*0.71*	*0.43*	*1.07*		*2.26*	
I-40	13		6.05	4.32	4.10		3.76	
100 °C	*0.87*		*2.04*	*0.51*	*1.13*		*1.58*	
I-40	15			4.31	4.10	3.84		
300 °C	*0.71*			*0.55*	*00.71*	*<0.33*		
IF-04	15	8.04		4.24	4.06		3.72	
RT	*1.19*	*0.40*		*0.64*	*0.96*		*0.63*	
IF-11	(15–9 Å)	only very broad bands					~3.7	
RT	(*1.4*)						*~1*	
IF-12							3.70	
RT							*0.67*	
IF-12		~9						
500 °C		*1.10*						
IF-13		~8.9					~3.7	
RT		*~0.6*					*~1.3*	
500 °C		(~8.8?)						
IF-14	~13		5.9				3.70	
RT	*1.18*		*0.83*				*3.01*	
IF-41	15	8.84		4.32	4.11		3.79	3.43
RT	*1.38*	*0.51*		*0.69*	*1.18*		*0.60*	*0.24*
IF-41	15	8.46	5.99	4.32	4.12	3.83–3.76?		
100 °C	*0.94*	*0.30*	*0.31*	*0.67*	*1.00*	*0.24*		
IF-41	15	8.12		4.30	4.08			
300 °C	*0.93*	*0.37*		*0.84*	*0.65*			

Table III. BET Surface Area, A; Ratio of the Pore Volume (V) at the Onset to the Pore Volume at the Upper Limite (V_t) of the Hysteresis Loop, V/V_t; Average Thickness of the Adsorbed Layer at the Onset of the Hysteresis Loop, t; $r_p = r_K + t$ for V or V_t; and Volume of Liquid N_2, V [a]

sample	A(BET), $m^2\ g^{-1}$	V/V_t, %	$t(V)$, Å	$r_p(V)$, Å	$r_p(V_t)$, Å	V, mL g^{-1}
I-24	67	47.2	5	13	70	0.030
I-20	78	66	5	13	70	0.034
I-40	122	70.5	8	40	120	0.044
IF-12	406	70.4	6	17	120	0.14
IF-04 (IF-41)	217	72.3	5	13	64	0.10
IF-13	408	77.2	6	16	64	0.14
I-42	263	85	5	13	64	0.11

[a] All samples calcined at 300 °C for 2 h.

(lower P/P_0) and V_t is the volume at the upper P/P_0, V/V_t is the relative contribution, to the pore volume, of the pores in the galleries existing between the silicate layers propped apart by the pillars. As shown by the numerical data in Table III and with the exception of sample I-24, more than two-thirds of the total pore volume, defined as V_t, is within galleries with radii between t and $r_p(V)$, or between ~6 and ~15 Å. The diameter, ϕ, of the Al_{13} pillar is on the order of 9 Å, namely, smaller than $2r_p$. Anchoring the pillars to the inverted silicon tetrahedra of the puckered silicate layer may account for the difference ($2r_p - \phi$), notwithstanding, as stated above, the significance of r_K at low P/P_0. From the results in Table III, it is clear that it would be meaningless to calculate a "pore size

Table IV. ^{29}Si NMR Data from Spectrum Deconvolution, Chemical Shifts, and Q^3 and Q^4 Contributions[a]

sample	T_{pret}, °C	$-\nu_A$	$-\nu_B$	% A	% B	A/B	spectrum
D-31	RT	100.7	108.5				
D-32	RT	98.8	108.9	68.4	31.6	2.16	
	500	99.3	108.7	36.8	63.2	0.58	
I-10	70	99.6	107.3	48.7	51.3	0.95	5a
	300	(100.4)	107.4	35.5	64.5	0.55	5b
I-20	RT	98	108	62.4	37.6	1.66	
	500	100	110	15.5	84.5	0.18	
I-40	100	101.7	108.9	47.1	52.9	0.89	5c
	300	(100.9)	108.5	37.8	62.2	0.60	5d
	500	(101)	108.5	32.2	67.8	0.47	5e
IF-41	RT	101.7	111.3	36.1	63.9	0.56	5g
	300	102.3	111.5	35.3	64.7	0.55	5h

[a] A designates the line at −98 to −102 ppm, attributable to Q^3(1OH) and/or Q^4(1Al) environments, B the line at −108 to −112 ppm, attributable to a Q^4(4Si) environment. Q^4(4Si) is a shorthand notation for $((SiO)_4Si)$, Q^4(1Al) for $((SiO)_3SiOAl)$ and Q^3 for $((SiO)_3SiOH)$.

distribution" from N_2 adsorption or desorption isotherms since more than two-thirds of the pore volume is in the P/P_0 region where the application of the Kelvin law is very questionable. The remaining one-third (or less) of the contribution to the pore volume is in mesopores with radii between ~15 and ~100 Å. These mesopores are most probably created by the delamination of the silicate layers consecutive to the alkylammonium deintercalation upon pillaring. With these concepts in mind, it is suggested that the higher the ratio V/V_t, the more ordered is the distribution of the pillars within the galleries. The disorder in this distribution and the interstratification of bridged and pillared domains account for the lack of constructive interferences in the XRD pattern and thus the lack of defined $0k0$ reflections.

In Table III, V is expressed in milliliters of liquid N_2 occluded in the galleries. For the last four samples, V is in the range reported for pillared clays.[6] There is no correlation between the intensity of the broad XRD band, with d spacing at ~15 Å, and the surface area.

The surface area, the pore volume (V), and, especially, the ratio V/V_t, considered as indicative of the contribution of the pillared galleries to the total volume of pores with radii ≤ 100 Å, are sensitive to many factors. Although we do not claim to have optimized the procedure for obtaining the most ordered pillared intercalates, several trends are already apparent. From Tables III and I, the following are clear: (i) R(Al), the nominal concentration of Al polymer (expressed in milliequivalents of Al^{3+}) per gram of starting material, must be on the order of 180. A lower R (such as that used for I-20) yields a low value of V. (ii) Increasing the temperature for Al intercalation to 90 °C yields the less ordered material (I-24). (iii) The pH maintained during the preparation of the ethylammonium precursors plays a role. For instance, I-40, whose precursor was prepared at pH ~ 5, has a V/V_t ratio and a V value significantly lower than that of I-42, whose precursor was prepared at pH = 2.5. In addition, upon heating for 2 h at 300 °C, I-42 loses 13% of its surface area measured after outgasing at 100 °C, whereas I-40 loses 34% of its initial surface area at 100 °C (Table I).

The titration curve of ethylamine into ethylammonium fluoride by HF does not show the steep pH drop observed for the formation of ethylammonium chloride. Instead, a plateau extending from pH ~ 6.5 to 6 is obtained. Therefore, the ethylammonium fluoride precursors were prepared at pHs between 5 and 6.5. As shown in Table I, the products obtained through indirect exchange of the ethylammonium fluoride intercalate yield generally the highest surface areas (from 230 to 490 m^2/g). These high surfaces, compatible with the generally low crystallinity observed by XRD, are also more stable under calcination (see sample IF-13) but seem to be very dependent on the conditions of the ethylammonium fluoride intercalation (amount of exces HF and washing procedure).

In addition (see Table III), IF-04, IF-12, and IF-13 have high V/V_t ratios. The chemical analysis of IF-41 (quasi-identical with IF-04) shows that some fluorine is introduced within the lattice.

Chemical Composition of the Intercalated Silicates. More informative formulas will be written using the results of the NMR analysis (see Discussion section and Table VI). However, it is worth noticing that a sample of the IF series was submitted to C, H, and N analysis to check the elimination of ethylammonium upon Al intercalation. Before contact with ACH, it contained 4.19% C, 2.12% H, and 2.51% N (theoretical values for a degree of exchange $2z = 0.27$, unhydrated sample: 4.30% C, 1.87% H, 2.51% N); after contact, the contents were down to 0.08% C, 0.60% H, and 0.08% N. Thus, almost all of the organic material had been removed from the solid (excess H is due to silanol groups).

SEM. Figure 10 shows scanning electron micrographs of HP, I-42, and IF-13. It is obvious that the pillared products have the same layered structures as HP. No alumina precipitates are observable in the pillared materials, and the particle sizes are similar for the three samples. The BET surface areas for HP, I-42, and IF-13 (calcined at 300 °C) are 24, 263, and 408 m^2/g, respectively. It seems evident that the large increase in surface area observed for the pillared materials is due to the intercalation of Al pillars, in agreement with the conclusions obtained from the N_2 adsorption–desorption isotherms.

^{29}Si MAS NMR. Selected spectra are shown in Figure 5. All recorded spectra were deconvoluted, and the results of these deconvolutions are presented in Table IV.

(a) Direct-Exchange Products. The one-pulse ^{29}Si spectrum obtained for D-32 after RT drying exhibits two lines at −98.8 and −108.9 ppm with respect to TMS. These lines are in the normal range for Q^3 and Q^4 environments, respectively. After calcination at 500 °C for 2 h, the spectrum is dominated by a strong line at −108.7 ppm with a shoulder at −99.3 ppm. Similar spectra were obtained for sample D-31.

(b) Indirect-Exchange Products. The spectra of sample I-10 after drying at 70 °C and calcining at 300 °C are reproduced in spectra a and b of Figure 5, respectively. The qualitative picture is comparable with the direct-exchange products; this is also the case for I-20 (not represented). However, the relative importance of the lines at ~ −100 and ~ −110 ppm in the dried samples is variable (see Table IV).

Sample I-40 also exhibits the same evolution between 70 and 300 °C. (Spectra c and d of Figure 5). Further

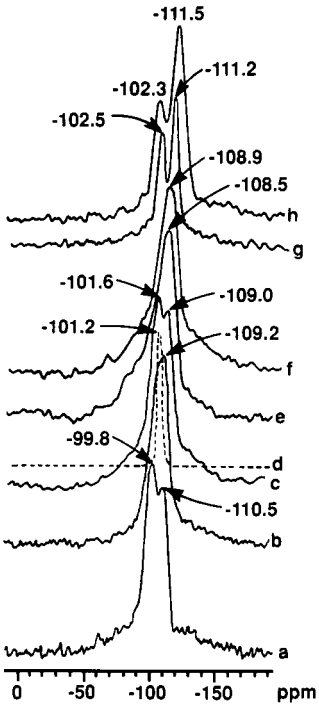

Figure 5. ^{29}Si solid-state MAS NMR spectrum (ν_L = 99.3 MHz, with proton decoupling) of (a) I-10 (indirect exchange of the ethylammonium chloride intercalate with Al_{13} solution), dried at 70 °C for 12 h; (b) I-10 calcined at 300 °C for 2 h; (c) I-40 (indirect exchange with ACH solution), dried at 100 °C for 12 h, and (d) with cross-polarization; (e) I-40, calcined at 300 °C for 2 h; (f) I-40, calcined at 500 °C for 2 h; (g) IF-41 (indirect exchange of the ethylammonium fluoride intercalate with ACH solution), after RT drying; and (h) IF-41, after 2 h calcination at 300 °C. Reference: TMS.

calcination at 500 °C for 2 h hardly modifies the spectrum (Figure 5e). In addition, the spectrum of the 70 °C dried sample was also recorded with cross-polarization and is shown in Figure 5f. It can be seen that only the peak at ~−100 ppm is observed under CP, with a reduced intensity and a slightly displaced maximum. This establishes that the ~−100 ppm line is partly due to silanol groups, while the Si species with resonance at ~−110 ppm has no proton neighbors.

Finally, spectra g and h of Figure 5 show the ^{29}Si NMR spectrum of a product of indirect exchange via ethylammonium fluoride intercalation, sample IF-41, at RT and after 300 °C calcination, respectively. The general features are similar to what is observed for the product of exchange via the ethylammonium chloride intercalate.

^{27}Al NMR. (a) Aluminum Polyhydroxy Polymer Solutions. The ^{27}Al high-resolution liquid NMR of pure $Al_{13}^{x+}Cl_x^-$ solution containing 0.1 M in total Al is shown in Figure 6a. Only one very sharp line is visible at +63 ppm relative to $Al(H_2O)_6^{3+}$, corresponding to tetrahedral AlO_4 in symmetrical coordination at the center of the Al_{13} polymer. Since no line is observed at ~0 ppm, it seems that very little $Al(H_2O)_6^{3+}$, if any, is present in the solution.

In contrast, in the case of the diluted and aged ACH solution containing 0.2 M total Al (Figure 6b), Al_{13} appears to be only a minor component. Its resonance is superimposed onto very broad, solidlike bands at ~8 and ~72 ppm, with another sharp component at 0 ppm; that spectrum is very similar to some obtained by Akitt and Farthing (ref 15—in particular, see the spectrum in their Figure 2a). Thus, it seems that ACH solutions contain

(15) Akitt, J. W.; Farthing, A. *J. Magn. Reson.* **1978**, *32*, 345.

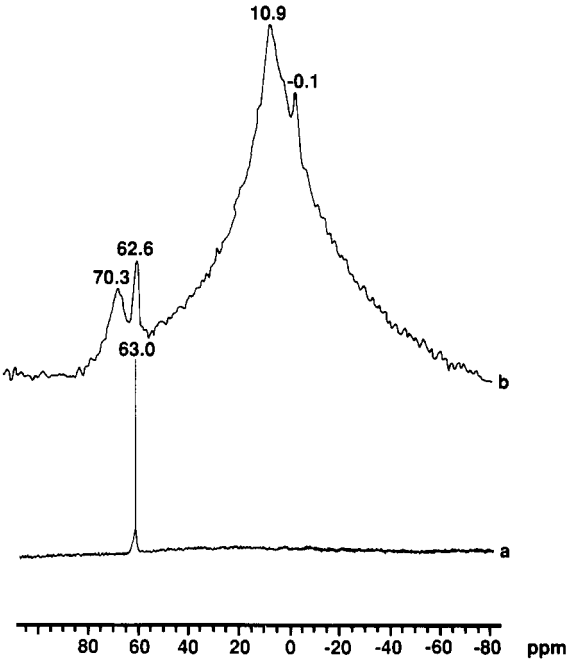

Figure 6. Liquid-state ^{27}Al NMR of (a) a "pure Al_{13}" solution (ν_L = 65.1 MHz) and (b) the ACH solution, after dissolution to 0.2 M and 2-h aging at 60 °C (ν_L = 130.3 MHz). Reference: $Al(H_2O)_6^{3+}$ in 0.1 M $AlCl_3$ solution.

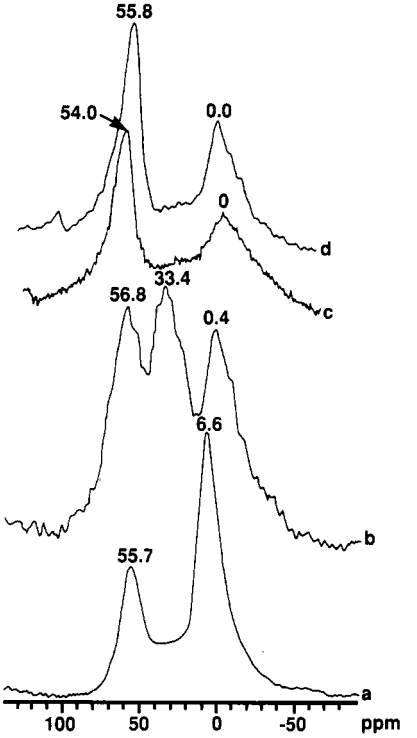

Figure 7. ^{27}Al solid-state MAS NMR spectrum (ν_L = 130.3 MHz) of (a) direct-exchange product D-32, dried at RT; (b) D-32, calcined at 300 °C for 2 h; (c) I-10, product of the indirect exchange of the ethylammonium chloride intercalate with Al_{13}, dried at 70 °C for 12 h; and (d) I-10, calcined at 300 °C for 2 h. Reference: $Al(H_2O)_6^{3+}$ in 0.1 M $AlCl_3$ solution.

important quantities of aluminum in species different from Al_{13}, a fact that is often overlooked.

(b) Direct-Exchange Products. The ^{27}Al MAS NMR spectra for one typical sample, D-32, are shown in Figure 7. After RT drying (Figure 7a), two bands are apparent at +55.7 and +6.6 ppm, with a relative intensity of 1:2. They are in the range of chemical shifts of tetrahedrally and octahedrally coordinated Al, respectively. After cal-

Table V. ^{27}Al NMR Spectra Deconvolution, Approximate Relative Intensities, and Positions of the Centers of Gravity of the Lines

sample	T_{pret}, °C	% Al^{IV}	% Al^{V}	% Al^{VI}	$\nu_{Al^{IV}}$	$\nu_{Al^{V}}$	$\nu_{Al^{VI}}$	spectrum
D-32	RT	34.9		64.1	55.7		6.6	7a
	500	26.9	45.0	28.1	56.8	33.4	0.4	7b
I-10	70	*a*			54.0		0	7c
	300	54.2		45.8	55.8		0	7d
I-20	RT	17.2	6	76.7	56.3	(~31)	4.9	8a
	500	27.2	9.9	62.8	56.9	32	4.1	8b
I-40	100	*a*			56	~31	4.4	8c
	300	39.1	35.7	25.1	54.8	~30	4.0	8d
	500	42	48.5	9.5	(56)	(31)	(0.8)	8e
IF-41	RT	18.7	8.3	72.9	55.7	30.3	6	9a
	300	18.7	42.7	38.6	53.4	30.9	4.2	9b

[a] Spectrum too broad to be deconvoluted. The species labeled Al^{V} may as well be assigned to distorted tetrahedral Al (see Discussion section). Values in parentheses are obtained from spectrum deconvolutions; the other correspond to observed peak maxima.

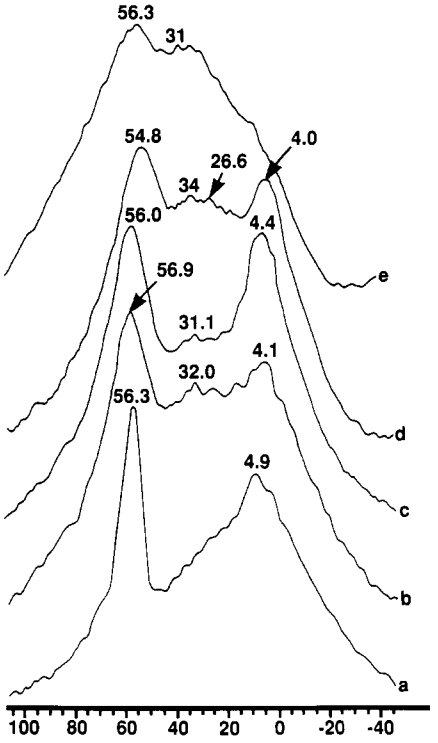

Figure 8. ^{27}Al solid-state MAS NMR spectrum (ν_L = 130.3 MHz) of (a) I-20, product of indirect exchange of the ethylammonium chloride intercalate with ACH, after RT drying; (b) I-20, after calcination at 500 °C for 2 h; (c) product of indirect exchange I-40, dried at 100 °C for 12 h; and (d) I-40, calcined at 300 °C for 2 h and (e) calcined at 500 °C for 2 h. Reference: $Al(H_2O)_6^{3+}$ in 0.1 M $AlCl_3$ solution.

cination at 500 °C for 2 h, important differences are apparent in the ^{27}Al NMR spectrum: we now observe three well-individualized bands at 56.8, 33.5, and 0.4 ppm (Figure 7b), with relative intensities of about 1:1.6:1. The assignment of the 33.5 ppm line is problematic: similar chemical shifts in steamed zeolites have been attributed to strongly distorted tetrahedral aluminum,[16] but a recent study of dehydrated kaolinites would suggest the possibility of pentacoordinated aluminum (ref 17 and references therein).

(c) Indirect-Exchange Products. ^{27}Al NMR spectra of samples I-10, I-20, I-40, and IF-41 are shown in Figures 7 and 8.

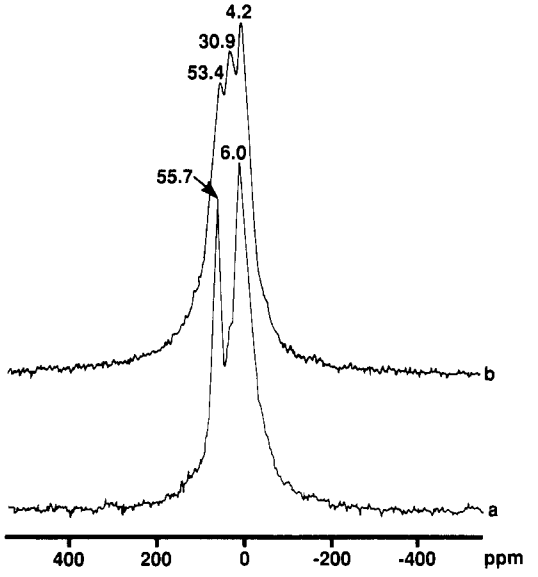

Figure 9. Broad-scan ^{27}Al solid-state MAS NMR spectrum (ν_L = 130.3 MHz) of (a) IF-41, product of indirect exchange of the ethylammonium fluoride intercalate with ACH solution, after RT drying; and (b) IF-41, calcined for 2 h at 300 °C. Reference: $Al(H_2O)_6^{3+}$ in 0.1 M $AlCl_3$ solution.

For sample I-10 (dried at 70 °C), the one-pulse ^{27}Al NMR spectrum contains two lines at about 54.0 and 0 ppm (Figure 7c); after calcining at 300 °C for 2 h (Figure 7d), these two lines are still present.

The ^{27}Al NMR spectrum of sample I-20 has two bands at 56.3 and 4.9 ppm, the latter asymmetrical (Figure 8a); after calcination at 500 °C for 2 h, the spectrum contains three lines at 56.9, ~32, and 4.1 ppm (Figure 8b).

For sample I-40, after drying at 100 °C for 2 h (Figure 8c), the spectrum already contains three lines at 56.0, 31.1 (weak), and 4.4 ppm; after calcining at 300 °C for 2 h (Figure 8d), the peak positions change only slightly (54.8, ~30, and 4.0 ppm, respectively) but the relative intensities are strongly modified. After calcination at 500 °C (Figure 8e), the ^{27}Al NMR spectrum is ill-resolved and dominated by a very broad feature; however, a line at 56 ppm is still discernible.

The ^{27}Al resonance spectra recorded for the samples obtained in monitoring the pH during the alkylammonium intercalation exhibit the same features as those observed for samples I-20, namely, lines at ~55 and ~0 ppm for RT dried samples and an additional line at about 29 ppm that is mainly observable after calcination at 300 °C. Semiquantitatively the ratio Al^{IV}/total Al is on the order of 40%. The picture for sample IF-41 is similar (Figure 9), except for the weaker overall intensity of the aluminum

(16) Samoson, A.; Lippmaa, E.; Engelhardt, G.; Lohse, U.; Jerschekewitz, H. G. *Chem. Phys. Lett.* **1986**, *134*, 589.
(17) Lambert, J.-F.; Millman, W. S.; Fripiat, J. J. *J. Am. Chem. Soc.* **1989**, *111*, 3517.

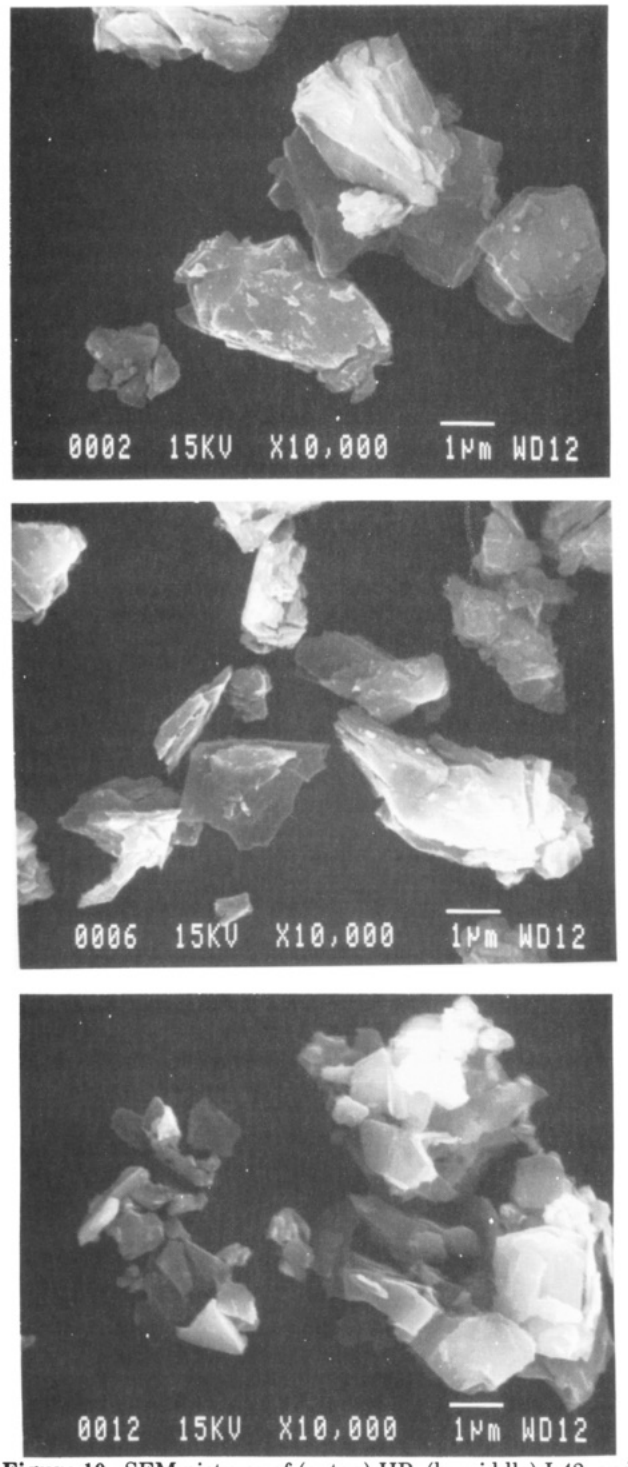

Figure 10. SEM pictures of (a, top) HP, (b, middle) I-42, and (c, bottom) IF-13.

signal, corroborating the smaller Al content from chemical analysis.

The ^{27}Al NMR results are summarized in Table V.

Discussion

As mentioned in the Introduction section, the present study was undertaken in the hope that topotactic intercalation of Al_{13} cations into the structure of $KHSi_2O_5$ would be possible, in a manner similar to what is observed for clay minerals. Alkylammonium intercalates were chosen as starting materials with the rationale that the already large separation of the oxide layers in these compounds[9,18] would make the interlayer space more easily accessible to the inorganic oligomers; the ethylammonium was selected in preference to longer alkyl chains, which might have given too stable intercalates, difficult to break down.

The 020 XRD reflections of both $KHSi_2O_5$ and the ethylammonium intercalate, observed at 6.32 and 8.7 Å, respectively, disappear upon contact with either ACH or Al_{13}, which indicates a loss of long-range order along the *b* axis; chemical analysis shows that only a small percentage of the initial K^+, or RNH_3^+, remains in the final products.

Therefore, our starting materials are indeed completely modified by reaction with the aluminum pillaring solutions. If, however, Al_{13} were intercalated in the interlayer space in a truly topotactic reaction, this would result in the observing of a well-characterized peak at high spacings in the X-ray diffractograms. In many spectra, a very broad band is observed around 15 Å, slightly higher than the sum of the layer thickness and the Al_{13} diameter, but it is never well-defined. Besides, the spectrum of RT dried products often exhibits peaks reminiscent of the hydrolyzed form,[9] which disappear upon heating. In contrast with the loss of order in the direction perpendicular to the layers, however, weak *h*0*l* reflections are present in the Al-containing products and subsist after calcination. We attributed them to the "collapsed phase" formed by regular siloxane-bridge formation from the theoretical $H_2Si_2O_5$ structure, and one of them is close to the 200 of the original $KHSi_2O5$: thus, the layer structure of the silica network is preserved to some extent.

Thus, we believe that at least two competing processes interfere with the intercalation of aluminum-containing species: first, the proton exchange of either K^+ or RNH_3^+ ions in moderately acidic solutions (ACH and Al_{13} solutions have pHs ranging between 3.7 and 4.3); second, accompanying the hydrolysis as proposed in ref 9, partial condensation of newly formed silanol groups in different layers to form siloxane bridges. The latter reaction explains the existence in aluminum-contacted products, not calcined, of a substantial (and variable) amount of Si atoms in a $Q^4(4Si)$ environment, while all Si atoms in the original structure were Q^3. The irregular alternating of collapsed and noncollapsed layers, or interstratification, explains the low intensity, large width, and thermal unstability of the 0*k*0 reflections.

These two undesirable side reactions certainly occur, but some other process must be at work too. Indeed, the large increases in surface area apparent from Table I could not be explained by hydrolysis/layer condensation only, since the products of acid hydrolysis of $KHSi_2O_5$, even under much more aggressive conditions, never have surface areas higher than 40 m^2/g. In particular, there is no extensive destruction of the lattice to form amorphous silicas or silicoaluminas, as evidenced by the preservation of *h*0*l* reflections. In addition, the analysis of the N_2 adsorption–desorption isotherm leads to the conclusion that, in the most favorable preparation procedures, galleries with openings between ~10 and ~30 Å (Table III) contribute to more than two-thirds of the volume of pores with radii ≤ 100 Å.

Also, chemical analysis indicates that the final products contain aluminum: thus, contact with aluminum polymers solutions stabilizes a high-surface form of the silicate. This cannot be due mainly to the coexistence in a physical mixture of low-surface hydrolyzed silica with a high-surface aluminum precipitate, since it would lead to unrealistically high values for the surface area of the latter.

Therefore, we are led to admit the existence of an interaction between Al and the silicate lattice. At this point,

(18) Lagaly, G. *Adv. Colloid Interface Sci.* **1979**, *11*, 105.

solid-state NMR is most helpful in clarifying the nature of this interaction.

Let us first consider ^{29}Si NMR results. One-pulse ^{29}Si MAS NMR spectra generally show two lines at about −100 ppm and about −108 to −110 ppm (Figure 5 and Table IV). As mentioned earlier, the line at ~ −108 ppm can be assigned to a $Q^4(4Si)$ silicon environment, i.e., $(Si–O)_4Si$. On the other hand, the line at −100 ppm could be assigned to two kinds of silicon sites, either a $Q^3(1OH)$ site, that is, a silanol group, or a $Q^4(1Al)$ environment, in which three of the oxygens of the SiO_4 unit are linked to Si and the fourth is linked to Al.[19]

Silanol groups are of course abundant in the hydrolyzed product.[9] For the Al-intercalated samples, we observed that the ~ −100 ppm peak was still present under cross-polarization but with a markedly weaker intensity. This indicates that there must be some contribution other than silanols. Also, it can be seen from Table IV that, although the relative intensity of the ~ −100 ppm line (line A in Table IV) decreases upon calcination (as expected if more silanols condense to form siloxane bridges), it has by no means disappeared even at 500 °C. In summary, line A probably consists of two components too close to be resolved under our operating conditions, one corresponding to $Q^4(1Al)$ and the other to $Q^3(1OH)$.

Thus, there is evidence for the formation of Si–O–Al bonds. Let us call such Si-linked Al "framework aluminum" by analogy with the nomenclature used for zeolites. There remain different possibilities: either framework Al (Al_F) simply replaces silicon in some (SiO_4) tetrahedra without altering the connectivity of the silicate layers or it is the result of condensation with dangling Si–O–H bonds between the layers and then it changes the dimensionality of the lattice from two- to three-dimensional. The first process (SiO_4 substitution) is very well-documented in zeolites.[20,21] However, if it occurred here to any appreciable extent, this would result in the formation of some Si atoms in a $Q^3(1Al)$ environment, with an expected line at ~ −90 ppm in the ^{29}Si spectra (such as in beidellite, ref 6). Besides, simple substitution could not account for the increase in surface area.

In the same way, the formation between successive layers of "short" pillars of the type $Si–O–Al^{IV}–O–Si$ would not result in sufficient layer separation to make the interlayer space available to adsorption. Therefore, we must represent the interlayer bonds as $Si–O–Al_F–(Al_{NF})–Al_F–O–Si$, where Al_F, according to our definition, is the framework aluminum and where Al_{NF} stands for nonframework alumina moieties. It follows that each Si in a $Q^4(1Al)$ environment corresponds to one framework Al. We may ask the question of the tetrahedral or octahedral coordination of this framework aluminum. Now, in beidellite, for example, silicon connected with an Al^{VI} of the octahedral layer has a resonance at −95 ppm,[6] which is not observed in our spectra, precluding the existence of a large number of $Si–O–Al^{VI}$ bonds: thus, framework aluminum is essentially tetrahedral.

The ^{27}Al MAS NMR spectra (Figures 6–8 and Table V) recorded at RT indicate the presence at least of tetrahedral (about 55–60 ppm chemical shift) and octahedral (about 0–10 ppm) aluminum. In addition, upon dehydroxylation, part of the octahedral aluminum transforms to a species with a chemical shift of about 30 ppm, which we may assign to either pentacoordinated[17] or strongly distorted tetracoordinated aluminum.[16] This line is particularly prominent in Figure 9b.

The width of the ^{27}Al NMR lines and their probable asymmetry renders a quantitative deconvolution of the spectra difficult. To give the orders of magnitude, however, for the sample before calcination, the ratios of Al^{IV}/Al^{VI} are between 1/3 and 1/2 (Table V). This does not correspond to the structure of the Al_{13} species, since in the $[Al_{13}O_4(OH)_{24}(H_2O)_{12}]^{7+}$ cation the ratio of Al^{IV}/Al^{VI} is 1/12. In addition, the position of the Al^{IV} resonance of Al_{13} in pillared beidellites is at about 62 ppm and that of Al^{IV} in a Q^3 silicon environment is at 69 ppm;[6] these values are noticeably higher than the maximum Al^{IV} shift observed in the present study. It would then seem likely that most of the observed Al^{IV} resonance is due to Si-bonded framework aluminum; as for the Al^{VI} and the Al^{V} resonances that appear following dehydroxylation of the latter, they would belong to non-framework aluminum, i.e., Al not directly connected to the Si framework although it contributes to the propping apart of the layers.

It is interesting to point out that the position of the Al^{VI} line changes considerably according to the solution used for pillaring. The maximum of the Al^{VI} line is at ~0 ppm in sample I-10, obtained from pure Al_{13} (Figure 7c), while it is at 4.8 ppm for I-20 (Figure 8a) and ~4.4 ppm for I-40 (Figure 8c), both of which were obtained from ACH solutions. However, in samples obtained in monitoring the pH during the alkylammonium intercalation, the Al^{VI} resonance is between 0 and 3 ppm in spite of the fact that ACH was used as the pillaring agent. Remember that the ^{27}Al NMR of the ACH solutions indicate that Al_{13} is only a minor component of it (Figure 6b) and that it contains both Al^{IV} and Al^{VI} in other polymeric species. The maximum of the Al^{VI} line is at ~10 ppm, which may signal the presence of partly polymerized products.[22] The role of such species in Al pillaring has been little investigated so far, and it seems that the degree of polymerization of ACH itself is affected by the local acidity in the gallery. The interpretation of the Al^{VI} resonance line would be also complicated by the possible contribution of alumina precipitated outside the silicate layers.

To summarize, the experimentally observed ^{27}Al and ^{29}Si NMR spectra can be explained by assuming that the gallery contains $Si–O–Al^{IV}$ linkages and that the resulting negative charges on the Al tetrahedra can be balanced by Al_{13} or other Al-containing polymeric cations. Thus, we suggest that the equilibrium

$$Al_{polymer} \rightleftarrows Al_{13} (\rightleftarrows ...) \rightleftarrows \text{dimer} \rightleftarrows Al^{3+}$$

is first displaced to the right, allowing Al^{IV} to be formed within the gallery, and that subsequently positive charges brought by the Al oligomers compensate the negative charges of the $Si–O–Al^{IV}$ framework, propping the silica layers apart and thus creating a permanent surface area. One must keep in mind that this process is competing with hydrolysis, layer condensation, and possibly even partial amorphization.

The above working hypotheses allow a more quantitative exploitation of NMR results, provided the overall chemical composition is known from the chemical analysis. First, Si can exist in three different environments, $Q^4(4Si)$, with a resonance at ~110 ppm (called line B in Table II), and $Q^4(1Al)$ or $Q^3(1OH)$, both with a resonance at around −100 ppm (line A). Let us define x as the fraction of Si in a

(19) Fyfe, C. A.; Thomas, J. M.; Klinowski, J.; Gobbi, G. *Angew. Chem., Int. Ed. Engl.* **1983**, *22*, 259.
(20) Johansson, G. *Acta Chem. Scand.* **1960**, *14*, 769.
(21) Chang, C. D.; Chu, C. T.-W.; Miale, J. N.; Bridger, R. F.; Calvert, R. B. *J. Am. Chem. Soc.* **1984**, *106*, 8143.
(22) Bottero, J. Y.; Axelos, M.; Tchoubar, D.; Cases, J. M.; Fripiat, J. J.; Fiessinger, F. *J. Colloid Interface Sci.* **1987**, *117*, 47.

Table VI. Characterization of Pillaring Species in Three Samples (after 300 °C Calcination)

sample	I-10	I-40	IF-41
structural formula	$(Al_{0.114}Si_2)^{IV}O_{3.87}$-$(OH)_{0.596}(Al_2O_3)_{0.0481}$	$(Al_{0.054}Si_2)^{IV}O_{3.73}$-$(OH)_{0.701}(Al_2O_3)_{0.0426}$	$(Al_{0.010}Si_2)^{IV}O_{3.644}$-$(OH)_{0.695}F_{0.048}$-$(Al_2O_3)_{0.0219}$
MW	136.26	133.4	129.72
no. of siloxane bridges per unit formula (2 Si)	1.29	1.26	1.29
A_{th},[a] m^2/g	287.8	308.4	300.4
measd A, m^2/g	97.1	122.5	218
charge density,[b] e/nm^2	1.75	0.79	0.16
$(Si/Al)^{IV}$	17.6	37	198
Al_F/Al_{NF}	1.18	0.63	0.23
surface occupied per Al pillar,[c] Å^2	45	48	41

[a] Theoretically available surface area, A_{th} = (theoretical total surface area)(1 − (no. of siloxane bridges)/2). [b] Charge density = (no. of Al_F)/A_{th}. [c] Surface occupied per Al pillar = (A_{th} − measured surface area)/(no. of Al_{NF}).

$Q^3(1OH)$ environment and y as the fraction in a $Q^4(1Al)$ environment. I_A and I_B, the normalized intensities of the two NMR lines ($I_A + I_B = 1$), can be computed from the results in Table IV and we have

$$I_A = x + y, \quad I_B = 1 - (x + y)$$

We have written the chemical compositions of our samples as $Al_zSi_2O_{4+1.15z}\cdot wH_2O$. Now deconvolution of ^{27}Al NMR spectra allows an estimate of the relative quantities of Al in different coordinations: $I_{Al^{IV}}$, $I_{Al^{V}}$, $I_{Al^{VI}}$.

Since we assumed that all tetrahedral Al were framework Al connected with one (and only one) Si in the $Q^4(1Al)$ environment, of which there are $2y$ per formula, we may write

$$I_{Al^{IV}} = 2y/z$$

whence we can also deduce the silanol groups content:

$$x = I_A - \frac{z}{2} I_{Al^{IV}}$$

Let us illustrate these calculations from the example of sample I-40. Here, we have $I_{Al^{IV}} = 0.391$, $I_A = 0.378$, $I_B = 1 - I_A = 0.622$, and $z = 0.14$. This yields $x = 0.35$ and $y = 0.027$, allowing us to rewrite the formula of I-40 as $(Al_{0.054}Si_2)^{IV}O_v(OH)_{2x}\cdot 0.0426Al_2O_3$, where Al_2O_3 represents the nonframework aluminum, namely, Al in 6-fold and 5-fold (or very distorted 4-fold) coordination. Electroneutrality of the proposed structure requires that $(3 \times 0.54 + 2 \times 4) = 2v + 2y$, so that $v = 3.73$ and the molecular weight is 133.4 g.

Now we know that there are $2I_4 = 1.256$ bridged Si atoms per formula. The unit cell area of the precursor compound $[KHSi_2O_5]_2$ is $ac = 36.67$ Å^2, and if this indicative value is taken for the pillared compound, the theoretical surface area developed by the fully delaminated layers would be 829 m^2/g. The real structure, however, is a random interstratification of collapsed layers (where the siloxane bridges prevent accessibility of the gallery space for adsorption) and layers propped apart by the aluminic pillars. If there are no remaining isolated silanols in the collapsed layers, the inaccessible area is 829 I_B = 520.6 m^2/g, leaving 308.4 m^2/g in the pillared layers; the difference with the observed value of 122.5 m^2/g, i.e., 185.9 m^2/g, must be occupied by the pillaring species. The area prevented can then be computed to be ~48 Å^2 per atom of nonframework (pillaring) aluminum.

The same kind of calculations have been effected for samples I-10 and IF-41 and are summarized in Table VI. Calculated values for the density of the lattice charge are in the range observed for smectites and pillared smectites, as are the areas occupied per pillar and the surface area per Al_{NF}.

One important difference with clay minerals is the origin of the layer charge in pillared silicas. We think that the original (and high) layer charge of $KHSi_2O_5$ has been completely neutralized by proton exchange, forming silanol groups; upon contact with Al-containing solutions, however, Al would react with SiOH in the interlayer gallery, resulting in a modification of the lattice dimensionality and the building up of a network with negative charges on the newly formed Al tetrahedra. In turn, these charges would be compensated by the uptake of cationic Al polymers.

In general, indirect exchanges yield higher surface areas than direct exchanges; the highest surface areas so far were obtained through indirect exchange of the intercalates obtained from ethylammonium fluorides. It has been suggested that fluorine replaces some silanol groups in the interlayer gallery, lowering the formation of Si–O–Al_F and subsequent Al polymer uptake, as evidenced by the lower Al content of fluorine-containing sample IF-41. However, an excess of HF in the ethylammonium fluoride solution can attack the silicate network, resulting in extensive amorphization. Indeed, in $KHSi_2O_5$ hydrolyzed in 1 N HF, a line at ~−160 ppm has been observed in the ^{29}Si spectrum, perhaps due to the existence of Si–F linkages. Thus, a balance must be found between the positive and the negative consequences of fluorine substitution. Nevertheless, the ethylammonium fluoride route can stabilize products with high surface areas and high V/V_t ratios (Table III).

At this point, it seems appropriate to reconsider the title of this paper and ask a fundamental question, namely, can we claim to have aluminum-pillared the silicic network of $KHSi_2O_5$, or have we just smeared amorphous, high-surface silicoalumina on a remaining core of unmodified siloxane-bridged silica layers? Obviously, the XRD data cannot discriminate between these possibilities. The broad reflection at around 15 Å, observed in the product of $KHSi_2O_5$ hydrolysis as well as in the Al-contacted materials, can be due to random interstratification of collapsed (siloxane-bridged) and expanded (silanol-bearing) layers, as well as of collapsed and pillared layers. In the same way, ^{29}Si and ^{27}Al NMR data could be interpreted in terms of amorphization of the external silicic layers into silicoaluminas. Even the continued observation of $h0l$ reflections cannot provide an unambiguous answer, since the amorphous material could coexist with the untransformed crystallite cores (notice, however, that positions of the stable peaks do not correspond, in general, to those of the hydrolysis product).

So far, the evidence for pillaring is indirect. First, if we explained our results in terms of silicate amorphization upon contact with Al solutions, the observed $h0l$ peaks should be expected to weaken with increasing contact times, which is not the case. The study of the N_2 adsorption–desorption isotherms and the scanning electron

micrographs in Figure 10 support the conclusion that pillaring results in the formation of galleries who's volume contributes mostly to the porosity of the material. Second, another argument is provided by data concerning the alkylammonium intercalates (used for indirect-exchange processes). Indeed, these products exhibit high order along the swelling axis, as evidenced by the strong $0k0$ reflections, and it is easy to show that the area covered by the intercalated alkylammoniums is very close to the theoretically calculated area available to the Al pillars (from Q^3/Q^4 ratios: cf. supra). By use of the experimentally observed degrees of exchange ($2z \simeq 0.3$ in $(RNH_3^+)_{2z}H_{2(1-x'-z)}Si_2O_{5-x'}\cdot yH_2O$) and assuming that the alkylammonium chains oriented perpendicular to the layers covering an area of 25 Å^2,[23] the surface area available for intercalation in the silicate network would be ~345 m^2/g. This value is close to those reported in Table VI. In addition, we have shown that, by using ethylammonium fluoride intercalates (where some of the gallery silanols are replaced with fluoride), the amount of Si–O–Al^{IV} and of nonframework aluminum is dramatically reduced. Thus, there are clear indications that pillaring occurs to a large extent in the interlayer gallery.

(23) Lambert, J.-F.; Deng, Z. Q.; d'Espinose, J.-B.; Fripiat, J. J. Surface energetics of the intercalation process of N-alkyl amines or ammoniums with $KTiNbO_5$. *J. Colloid Interface Sci.* **1989**, *132*, 337.

Conclusion

$KHSi_2O_5$ and its intercalation products have been exchanged with solutions containing Al polyhydroxy polymers.

During the exchange process, three competing reactions may happen, namely, (1) hydrolysis of the solid with partial delamination and, in unfavorable cases, amorphization; (2) condensation of hydrolyzed layers with siloxane bridge formation; (3) pillaring by aluminum polymer cations.

In spite of this competition, Al pillaring is most probably extensive enough that high surface areas can be obtained without noticeable destruction of the lattice; an alternate explanation in terms of bulk amorphization cannot be definitely ruled out, but there exist considerable indirect evidence to make this explanation rather unlikely.

These high surface area products are stable at least until 300 °C for most exchange products, and preliminary work on ethylammonium fluoride intercalation-mediated ACH exchange indicates that they could be stable up to 500 °C. The intercalation process seems to proceed through initial grafting of Al^{IV} in the interlayer gallery, followed by charge compensation by Al-containing polymers.

Acknowledgment. An NSF grant (DIR-8719808) and an NIH grant (RR04095), which have partly supported the purchase of the GN-500 NMR instrument, are gratefully acknowledged. We thank J. Baken for the SEM pictures.

Water-Soluble Self-Doped 3-Substituted Polypyrroles

E. E. Havinga,*,† W. ten Hoeve,‡ E. W. Meijer,*,†,§ and H. Wynberg‡

Philips Research Laboratories, PO Box 80000, 5600 JA Eindhoven, The Netherlands, and Laboratory of Organic Chemistry, State University, Groningen, The Netherlands

Received July 7, 1989

The preparation of sodium salts of 3-alkylsulfonate pyrroles with various lengths of the alkyl chain (propyl-, butyl-, and hexylsulfonate) and their electrochemical polymerization to poly(3-alkylsulfonate pyrroles) are described. The low oxidation potential of the monomers allows a direct oxidative electrochemical polymerization, without additional conduction salts. The experimental conditions provide, for the first time, solid evidence of the existence of self-doped conducting polypyrroles. The polymers are characterized by spectroscopy (FTIR, UV–vis–NIR, ESR, ^{1}H NMR in D_2O solution), X-ray diffraction, cyclic voltammetry, and elemental analyses. The covalently attached sulfonate groups act as counterions for the charged backbone. The charge carriers are mainly spinless bipolarons. The conductivities are in the range $0.5–10^{-3}$ S/cm, the lower value referring to the hexyl chain. Indications are given for deviations from planarity of the main chain. The substituted polypyrroles are water soluble in the self-doped state. ^{1}H NMR spectra of the aqueous solutions of self-doped polymers are discussed.

Introduction

Extended conjugated polymers can, in general, be transformed into conducting materials by doping.[1] In the doping procedure, a reduction (to n-type doping) or oxidation (to p-type doping) yields highly charged polymer backbones. The charges are neutralized by counterions. In all traditional conducting polymers the counterions are absent in the neutral polymer and have to be injected into the polymer to provide doping. The doping process is often reversible, and the counterions or other neutralizing ions can move in and out many times. In self-doped conducting polymers, however, the counterions are covalently attached to the polymer backbone. The concept of self-dope of conducting polymers has been introduced by Patil et al.[2] In contradistinction with other doped polymers, dedoping of these self-doped polymers cannot be obtained by outdiffusion of the counterions but should be performed by in-diffusion of foreign cations. Moreover, the polymers in the self-doped state proved to be slightly soluble in water.[3]

The first-reported self-doped polymers were poly(3-alkylsulfonate thiophenes) **1a,b**, obtained by hydrolysis of

† Philips Research Laboratories.
‡ University of Groningen.
§ Present address: DSM Research, PO Box 18, 6160 MD Geleen, The Netherlands.

(1) See, e.g.: *Handbook of Conducting Polymers*; Skotheim, T. A., Ed.; Marcel Dekker: New York, 1986; Vol. 1 and 2.
(2) Patil, A. O.; Ikenoue, Y.; Basescu, N.; Colneri, N.; Chen, J.; Wudl, F.; Heeger, A. J. *Synth. Met.* **1987**, *20*, 151.
(3) Patil, A. O.; Ikenoue, Y.; Wudl, F.; Heeger, A. J. *J. Am. Chem. Soc.* **1987**, *109*, 1858.

0897-4756/89/2801-0650$01.50/0